Advanced Materials Research *Online: 2014-08-11*
ISSN: 1662-8985, Vol. 996, pp 556-561
doi:10.4028/www.scientific.net/AMR.996.556

Estimation of Cross-Sectional Residual Stress Distribution on Hardened Layer of Carburized Chromium-Molybdenum Steel by Electron Backscattering Diffraction Method

Yoshihisa Sakaida[1, *], Tomohito Inayama[2] and Shigeki Yashiro[1]

[1] Dept. of Mech. Eng, Shizuoka University, Naka-ku, Hamamatsu 432-8561, Japan

[2] Grad school of Eng, Shizuoka University, Japan

* Corresponding author: tysakai@ipc.shizuoka.ac.jp

Keywords: Carburizing, Quenching, Hardened Layer, Electron Backscattering Diffraction Method, Kernel Average Misorientation, Residual Stress, Chromium-Molybdenum Steel, Case Depth

Abstract. A chromium–molybdenum steel composed of 0.20 mass% carbon was used as a raw material. Three kinds of specimens having different case depths were made by carburizing and quenching. Using the scanning electron microscope, the crystallographic information was measured on the cross-sectional hardened layer by EBSD (electron backscattering diffraction) technique. The KAM (kernel average misorientation, Θ) maps were calculated from the carburized surface to the interior below the case depth of each specimen. The change in the area-average values, Θ_{mean}, of the KAM maps of each specimen was compared to the case depth and the cross-sectional residual stress distribution measured by X-ray. As a result, the area-average of the hardened layer was larger than that of the interior of specimen after quenching. The estimated depth of the increment in the Θ_{mean} was found to accord to the case depth and be proportional to the depth in which large compressive residual stress was distributed on the gradually polished surface. Therefore, both the case depth and eigen strain distribution that induce the compressive residual stress can be indirectly evaluated by electron backscattering diffraction method.

Introduction

The surface of the chromium–molybdenum steel parts used for transport vehicles are improved by the gas carburizing process. This heat treatment including oil quenching leads to the hardened layer and thermal compressive residual stresses near the hardened surface [1-3]. The hardened layer can be evaluated by measuring the cross-sectional hardness. The residual stress field in the heat treated parts can be measured experimentally by X-ray [1,3] or neutron stress measurement [1,2]. The hardened layer and the compressive residual stresses are generated by the martensitic transformation during quenching and the concurrent transformation plasticity [4].

Recently, the EBSD (electron backscattering diffraction) technique has been successfully applied to investigate the amount of plastic strains [5] subjected to ductile steel [6-9] or quenched steel [10, 11]. The area-average of the KAM (kernel average misorientation) maps calculated from the EBSD patterns could represent the amount of macroscopic plastic strains and the hardness. In those KAM calculations, it was necessary to define a threshold angle above which neighboring points were considered to belong to neighboring grains and were omited in the calculation. In general, a threshold angle would be set from 2 to 5° [5-11]. However this techinique could not be applied to the mixture of multiphases such as bainite and martensite phases. In our previous study [12], two kinds of specimens having different case depths were made by carburizing and quenching. To apply EBSD technique to the indirect estimation of macroscopic eigen strain distiribution induced by carburizing process, an appropriate threshold angle for calculating the area-average of KAM maps was examined. As a result, the depth in that compressive residual stresses existed was found to be evaluable by setting the threshold angle to 60° [12]. In this study, three kinds of carburized and quenched specimens were prepared. The case depth and the residual stress distribution near the carburized surfaces of these specimens were experimentally measured, and were compared to the area-average change of the KAM maps. The validity of our proposed indirect estimation was examined.

Experimental Procedure

Materials and Specimens. The initial material was a chromium–molybdenum steel, SCM420H, composed of 0.20 mass% C, 1.02 mass% Cr, and 0.17 mass % Mo. Young's modulus and Poisson's ratio of the initial material before carburizing were $E = 204$ GPa and $\nu = 0.27$, respectively. Four kinds of rectangular specimens were used, as shown in Fig. 1. The specimens, QC1 and AN, were cut from the blocks before and after the carburizing process. One block was carburized at 900 °C in a carrier gas and quenched at 850 °C in an oil bath, the other one was annealed at 620 °C for two hours and normalized at 900 °C for one hour. The specimens, QC2 and QC3, were cut from two hollow cylinders with an annular U-notch [2]. These cylinder were carburized at 900 and 950 °C in a carrier gas and quenched at 850 and 950 °C in an oil bath, respectively.

Measurement of EBSD Patterns. The EBSD patterns were observed using the thermal field emission scanning electron microscope (JSM-7001F, JEOL Ltd, Japan) with the orientation imaging microscopy (OIM, TSL solutions, Japan), as shown in Fig. 2. The crystallographic orientation was determined by the electron backscattering diffraction method. The kernel average misorientation, Θ, was estimated as,

$$\Theta = \frac{1}{6}\sum_{i=1}^{6}\theta_{Fi} \ , \tag{1}$$

where θ_{Fi} is a local misorientation between measuring and neighboring points. In this study, the area-average values, Θ_{mean}, of every 100 μm from the carburized surface to the interior along the z-direction of each specimen were calculated. The width of the y-direction for calculating the area-average value was more than 100 μm. The change in the area-average, Θ_{mean}, was compared to the case depth and the cross-sectional residual stress distribution measured by X-ray.

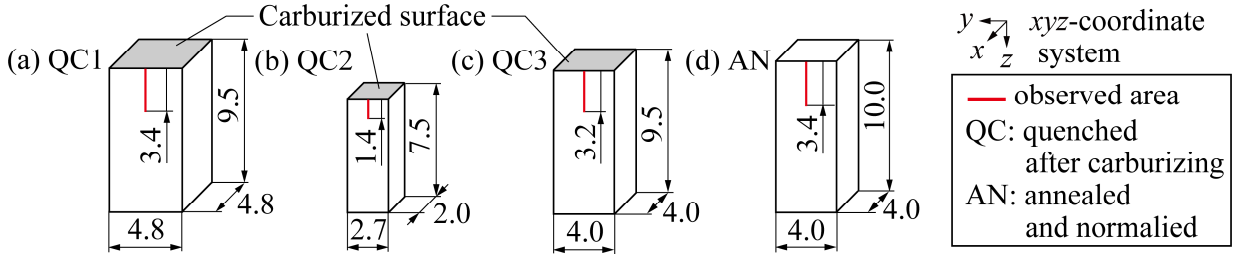

Fig. 1 Cut specimens and the definition of the coordinate system.

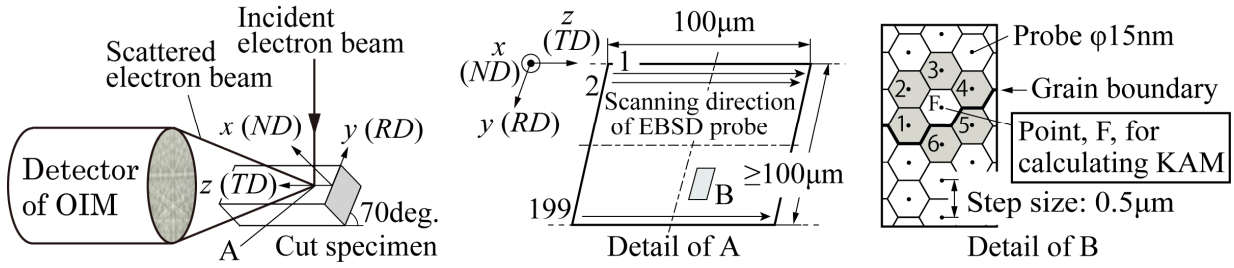

(a) EBSD patterns (b) area-average, Θ_{mean} (c) calculation of KAM

Fig. 2 Measurement of kernel average misorientations and area-average using OIM.

Determination of Case Depth. After quenching, the carbon content and hardness gradients of the cut specimens were measured to determine the case depth. The carbon content was measured by an electron probe microanalyzer and evaluated using the standard carbon steel specimens with known carbon content. The hardness was measured by a micro Vickers hardness tester. The indentation load and holding time were 2.9 N and 15 s, respectively. The total case depths were determined in reference to the Japanese Industrial Standard, JIS G 0557.

Measurement of Residual Stress Distribution. The residual stress distribution from the carburized surface to the interior was measured by the conventional $\sin^2\psi$ method with Ω-goniometer. Table 1

summarizes X-ray stress measurement conditions. In this study, the diffraction for Fe-211 reflection of ferrite or maritensite was used. Table 2 summarizes X-ray elastic constants, E_X and ν_X, before and after the carburizing process that were determined experimentally [13]. X-ray stress measurement was repeated by gradually removing the hardened layer by means of an electrolytic polishing.

Table 1 Stress measurement conditions.

Characteristic X-ray	Cr-Kα
Tube voltage [kV]	30
Tube current [mA]	8
Diffraction	αFe-211 martensite-211
Irradiated area	2 mm squares
Detector	PSPC (Fixed ψ_0)

Table 2 X-ray elastic constants, $E_X/(1+\nu_X)$ and E_X/ν_X, before and after the carburizing process [13].

	$E_X/(1+\nu_X)$ [GPa]	E_X/ν_X [GPa]
Before carburizing	167.5 ± 2.0	790.5 ± 58.4
Under carburized surface	194.6 ± 3.8	897.0 ± 41.9
Under decarburized layer	205.8 ± 6.2	1001.2 ± 36.0
Interior below case depth	176.6 ± 4.5	866.4 ± 15.3

Results and Discussion

Microstructures, Hardness and Carbon Content Gradients of Specimens. Figure 3 shows the carbon content gradients of carburized specimens, QC1, QC2 and QC3. In contrast to the base material with 0.20 mass% C, the carbon content gradients were observed near the carburized surfaces. The surface carbon content of specimen QC1 was smaller than those of specimens, QC2 and QC3. The carbon contents of three specimens plateaued at z = 2.6, 1.0 and 2.8 mm, respectively. Figure 4 shows the typical microstructures before and after the carburizing process. The microstructure of initial material was composed of ferrite and pearlite structures. On the other hand, as the distance from the surface increased, the microstructure after the carburizing process changed from the martensite to the bainite structures.

Figure 5 shows the Vickers hardness gradients of carburized specimens, QC1, QC2 and QC3. The hardness gradients caused by martensitic transformation were also observed near the carburized surfaces. Total case depths, d_{total}, of three specimens were found to be about 1.9, 0.8 and 2.2 mm, respectively.

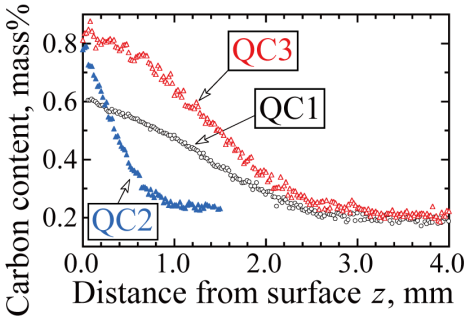

Fig. 3 Carbon content gradients after carburizing process.

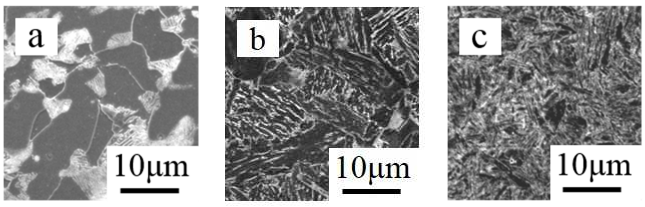

Fig. 4 Typical cross-sectional microstructures of specimens before and after carburizing process. (a) Specimen AN, (b) Interior of the carburized specimen QC3, and (c) Under the carburized surface of specimen QC3.

IPF (Inverse Pole Figure) Map and KAM (Kernel average Misorientation) Distribution. Figure 6 shows the typical IPF (inverse pole figure) map of specimen AN. Figure 7 shows the continuous inverse pole figure measured from the carburized surface to the interior of the specimen QC2. As mentioned above, in the case of specimen AN, the inverse pole figure corresponding to pro-eutectoid ferrite was observed, whereas in the case of specimen QC2, the subgranular inverse pole figure corresponding to martensite was observed near the carburized surface. This shows that the old austenite grains were transformed into some small martensite grains. In the interior below the case depth, the inverse pole figure corresponding to bainite was observed. Within the carburized layer, the

mixture of martensite and bainite grains was observed. The volume fraction of martensite phase decreased as the distance from the carburized surface increased.

Figure 8 shows the KAM distributions estimated from the measured IPF maps of the carburized specimens. The KAM distribution under the carburized surface was quite different from that of the interior below the case depth. Although the carbon content and hardness gradients differed from one another, the KAM distributions under the carburized surface were similar to one another. Therefore, by setting the threshold angle to 60°, the KAM maps are meaningful data for the mixture of martensite and bainite grains.

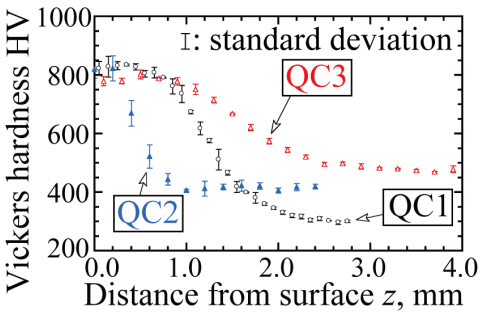

Fig. 5 Vickers hardness gradients after carburizing process.

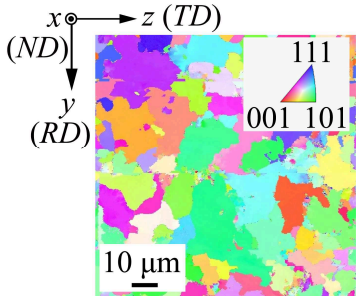

Fig. 6 Typical inverse pole figure of specimen AN.

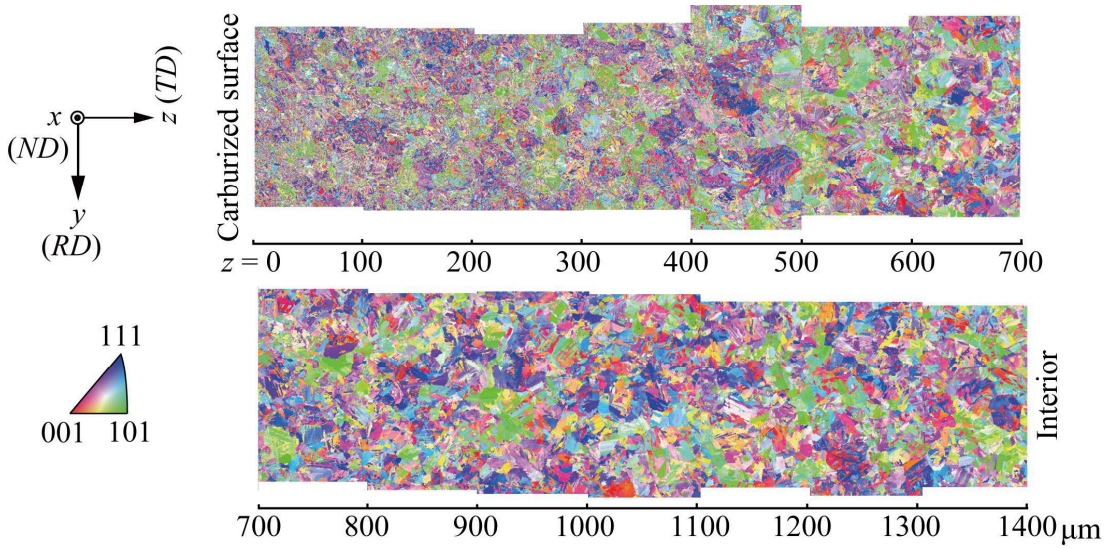

Fig. 7 The continuous inverse pole figure measured from the carburized surface to the interior along the z-direction of the specimen QC2. In this study, the grain tolerance angle = 5°.

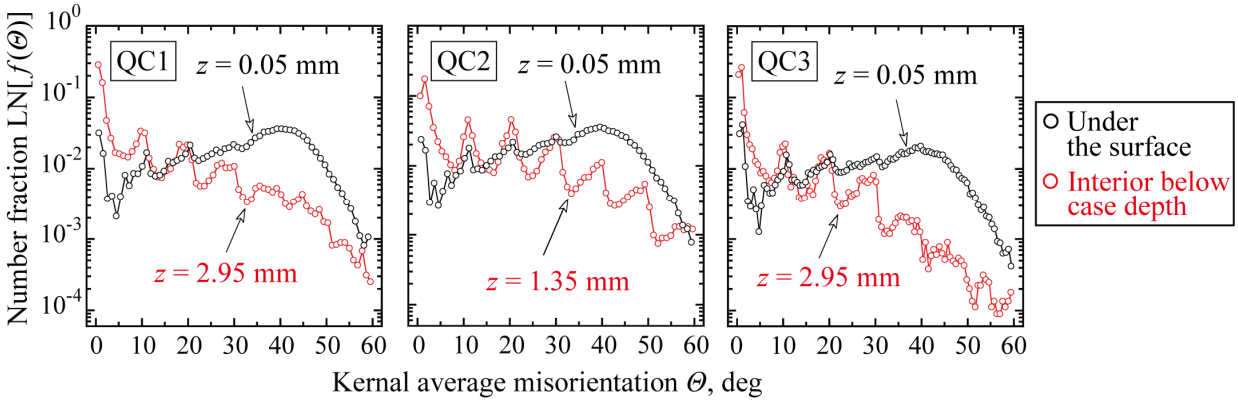

Fig. 8 Kernel average misorientation distributions of the specimens, QC1, QC2 and QC3.

Estimation of Case Depth and Residual Stress Distribution Using Area-Average of KAM Maps.

Figure 9 shows the changes in the area-average values, Θ_{mean}, of specimens, QC1, QC2 and QC3 in contrast to the initial base material specimen AN. The plateaued depths, d_{KAM}, in the area-average of three carburized specimens were 1.9, 0.8 and 2.0 mm, respectively. The d_{KAM} of each specimen was found to be almost equal to the total case depth, d_{total}.

Figures 10, 11 and 12 show a comparison between the residual stress and the Θ_{mean} distributions of each specimen. In these figures, the in-plane principal residual stresses, σ_1 and σ_2, were measured on the gradually polished surface. These residual stresses arise from eigen strains induced by the carburizing process [4]. The actual magnitude and direction of residual stress could not be predicted directly from the Θ_{mean} distribution because the Θ_{mean} profile differed from the residual stress distribution profile. But the decline in the compressive residual stress relatively accord with that in the area-average, Θ_{mean}. The depths, d_{res}, at which the compressive residual stress of three specimens plateaued were 2.6, 1.0 and 2.8 mm, respectively. The d_{res} of each specimen was found to be deeper than the d_{KAM}.

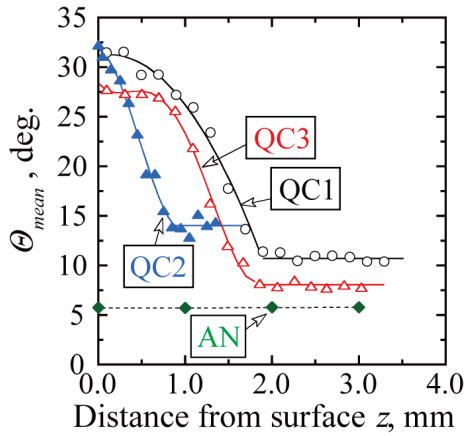

Fig. 9 Changes in the area-average, Θ_{mean}, of specimens QC1, QC2 and QC3.

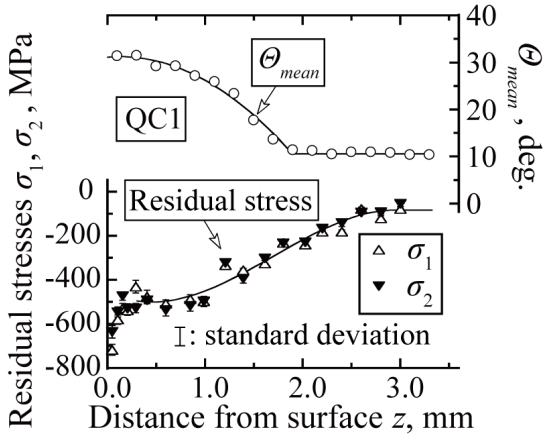

Fig. 10 Comparison between the residual stress and the Θ_{mean} distributions of specimen QC1.

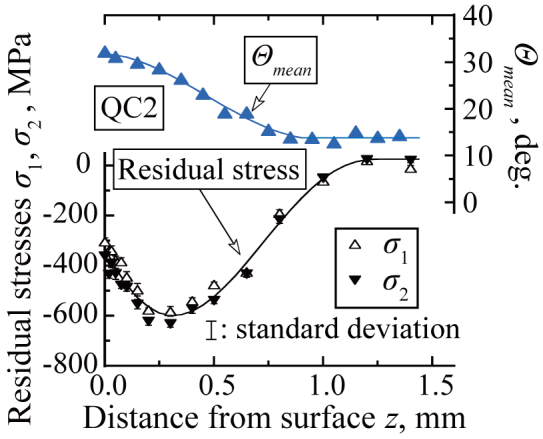

Fig. 11 Comparison between the residual stress and the Θ_{mean} distributions of specimen QC2.

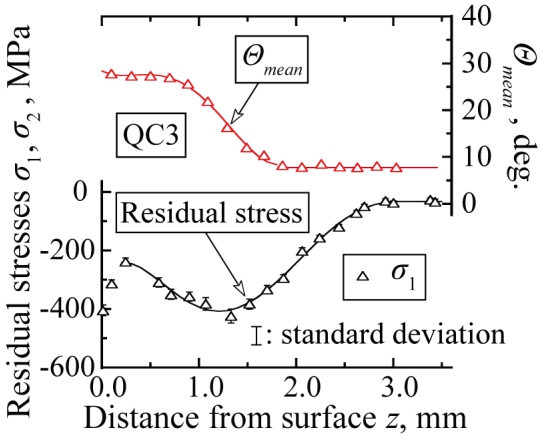

Fig. 12 Comparison between the residual stress and the Θ_{mean} distributions of specimen QC3.

Figure 13 shows the d_{total} *vs.* d_{KAM} and d_{res} *vs.* d_{KAM} relations for three carburized specimens. In this figure, two regression lines were derived by a least square method. Good linear correlations that passed through the origin were observed. In the case of the carburized chromium–molybdenum steel, the total case depth and the plateaued depth in residual stress can be predicted as,

$$d_{total} = 1.05\, d_{KAM}, \tag{2}$$

$$d_{res} = 1.49\, d_{KAM}. \quad (3)$$

In the case that the threshold angle is 60°, the increment of the area-average values represents the amount of volume expansion of martensite phase. Therefore, the case depth, d_{total}, is almost equal to the d_{KAM}. On the other hand, the d_{res}, at which the compressive residual stress plateaus, depends on both the volume expansion mismatch caused by martensitic transformation and the resulting plastic deformation of bainite phase. It is thought that the the d_{KAM} shortened than the d_{res}. It should be noted that the case depth and the area of concentrated eigen strain within the mixture of martensite and bainite grains are predictable by the proposed method.

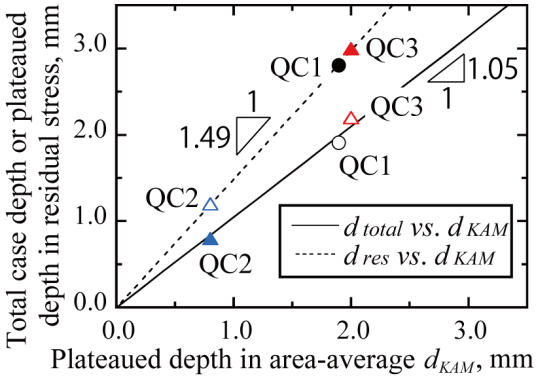

Fig.13 The d_{total} and d_{res} of the carburized specimens as a function of the d_{KAM}.

Conclusions

(1) The KAM distribution under the carburized surface was quite different from that of the interior below the case depth. By setting the threshold angle to 60°, the KAM maps are meaningful data for the mixture of martensite and bainite grains.

(2) The case depth and the plateaued depth in the compressive residual stress near the carburized surface are predictable by calculating the area-average of the KAM maps. In this study, the total case depth of carburized chromium–molybdenum steel is equal to the plateaued depth in the area-average. Furthermore, the plateaued depth in the compressive residual stress measured by X-ray is approximately 1.5 times as large as the plateaued depth in the area-average.

Acknowledgment

This study was supported by Grant-in-Aid for Scientific Researches (C), No. 24560095. The authors thank T. Murai (graduate student of Shizuoka Univ.) for experimental support.

References

[1] Y. Sakaida, M.Kawauchi, T.shobu, J. Soc. Mater. Sci. Jpn. 60-7 (2011) 649 -654.

[2] Y. Sakaida, T.Serizawa, M.Manzanka, J. Soc. Mater. Sci. Jpn. 60-7 (2011) 630-635.

[3] Y. Sakaida, S. Yamashita and M. Manzanka, Mater. Sci. Forum 681 (2011) 346-351.

[4] T. Inoue, Acta Mech. 214 (2010) 17-30.

[5] S. I. Wright, M. M. Nowell and D. P. Field, Microscopy and Microanalysis. 17 (2011) 316-329.

[6] H.Kimura, Y.Wang, Y.Akiniwa, K.Tanaka, Trans. Jpn. Soc. Mech. Eng. 71-A, (2005) 1722-1728.

[7]N.Nagashima, M.Hayakawa, Trans. Jpn. Soc. Mech. Eng. 79-A (2013) 23-33.

[8]K.Sasaki, M.Kamaya, T.Miura, K.Fukuya, Jpn. Inst. Metals, 74-7 (2010) 467-474.

[9]M. Kawakubo and M. Kamaya, Trans. Atomic Energy Soc. Jpn. 9-2 (2010) 166-173.

[10] S.Morooka, Y.Tomota, Y.Adachi, S.Morito, T.Kamiyama, Tetsu-to-Hagane 94-8 (2008) 43-50.

[11] K. Fujiyama, K. Mori, D. Kaneko, T. Matsunaga and H. Kimachi, Trans. Jpn. Soc. Mech. Eng. 74-A (2008) 323-328.

[12] Y. Sakaida, T. Inayama and S. Yashiro, J. Soc. Mater. Sci. Jpn. 63-7 (2014) in press.

[13] Y. Sakaida, S. Yashiro and H. Yoshida, J. Soc. Mater. Sci. Jpn. 62-5 (2013) 335 -341.